Chemistry Europe
European Chemical Societies Publishing

WILEY VCH

Excellence in Chemistry Research

Announcing our new flagship journal

- Gold Open Access
- Publishing charges waived
- Preprints welcome
- Edited by active scientists

Meet the Editors of *ChemistryEurope*

Luisa De Cola
Università degli Studi di Milano Statale, Italy

Ive Hermans
University of Wisconsin-Madison, USA

Ken Tanaka
Tokyo Institute of Technology, Japan

ChemPubSoc Europe

DOI: 10.1002/cssc.201701027

CHEMSUSCHEM Full Papers

High Efficiency $MAPbI_3$ Perovskite Solar Cell Using a Pure Thin Film of Polyoxometalate as Scaffold Layer

Mohammad Khaledi Sardashti,[a] Mahmoud Zendehdel,*[b] Narges Yaghoobi Nia,[c] Davud Karimian,[b] and Mohammad Sheikhi[d]

Here, we successfully used a pure layer of $[SiW_{11}O_{39}]^{8-}$ polyoxometalate (POM) structure as a thin-film scaffold layer for $CH_3NH_3PbI_3$-based perovskite solar cells (PSCs). A smooth nanoporous surface of POM causes outstanding improvement of the photocurrent density, external quantum efficiency (EQE), and overall efficiency of the PSCs compared to mesoporous TiO_2 (mp-TiO_2) as scaffold layer. Average power conversion efficiency (PCE) values of 15.5% with the champion device showing 16.3% could be achieved by using POM and a sequential deposition method with the perovskite layer. Furthermore, modified and defect-free POM/perovskite interface led to elimination of the anomalous hysteresis in the current–voltage curves. The open-circuit voltage decay study shows promising decrease of the electron recombination in the POM-based PSCs, which is also related to the modification of the POM/perovskite interface and higher electron transport inside the POM layer.

Introduction

Perovskite solar cells (PSCs) are a new class of emerging thin-film photovoltaic devices that could efficiently convert sunlight energy into electricity. The fabrication of efficient hybrid organic–inorganic perovskite thin-films based on $CH_3NH_3PbI_3$ ($MAPbI_3$) started in 2012.[1,2] These could be synthesized by low-temperature solution-based processes and have received special attention as a promising class of low-cost and high-efficiency photovoltaic devices. Owing to the excellent optoelectronic properties of thin-film solar cells based on $MAPbI_3$ perovskite and their mixed perovskites (cation-mixed and halide-mixed perovskites), such as sharp absorption edges[3] and large absorption coefficients[4] owed to their direct-gap character[5,6] and long carrier diffusion,[7,8] a rapid increase in power conversion efficiency (PCE), now exceeding 22.1%,[9] has been achieved.

PSCs have been regularly been designed using a mesoporous scaffold and layer-by-layer thin-film architecture of different components. The layers composed of transparent conductive oxide (TCO)-coated glass, regularly fluorine-doped tin oxide (FTO); an electron transport/selective layer (ETL), often in the form of a mesoporous scaffold of different thicknesses; the perovskite material, either infiltrated in the mesoporous scaffold or as a ''capping'' layer atop the ETL; and a hole transport/selective layer (HTL) with a metal contact as counter electrode. In PSCs, exciton formation can occur by injection of photogenerated electrons into the ETL and injection of holes into the HTL. Accordingly, free electrons created near the perovskite/HTL interface have to diffuse through the entire width of the absorber layer before being extracted at the ETL/perovskite interface, with increased chances of recombination. Similar cogitation applies to the holes near the ETL/perovskite interface. Recent reports demonstrated that both events (electron injection and hole injection in the respective transporting layers) occur in a similar timescale.[10] Edri and et al. studied the mechanism of charge separation applying direct measurement of electron-beam-induced current profiles of cross-sections of PSCs. These experiments revealed that the current enhances in regions close to the ETL/perovskite and perovskite/HTL interfaces, which indicates efficient electron and hole extraction near these interfaces, respectively, with electron-extraction efficiency somewhat higher than that of holes.[11] Thus, $MAPbI_3$ provides ambipolar transport and shows both electron-diffusion length and hole-diffusion length exceeding 1 μm.[10,12] Nevertheless, selective contacts are important to have stable, highly efficient devices with reduced recombination.[13]

[a] Dr. M. K. Sardashti
Department of Chemistry, Faculty of Sciences
Sharekord Branch, Islamic Azad University
Shahrekord 88137-33395 (Iran)

[b] Dr. M. Zendehdel, Dr. D. Karimian
K.S.R.I. (Kimia Solar Research Institute)
Kimia Solar Company
Isfahan 87137-45868 (Iran)
E-mail: mzzendehdel@gmail.com
m.zendehdel@kimiasolar.com

[c] Dr. N. Y. Nia
Centre for Hybrid and Organic Solar Energy (CHOSE)
University of Rome Tor Vergata
via del Politecnico 1, Rome 00133 (Italy)

[d] Dr. M. Sheikhi
S.E.M.C.O. (Iranian Strategic Energy and Carbon Management Company)
Tehran 14747-84549 (Iran)

Supporting Information for this article can be found under: https://doi.org/10.1002/cssc.201701027.

This publication is part of dual Special Issues on "Perovskite Optoelectronics", published in *ChemSusChem* and *Energy Technology*. Please visit the *ChemSusChem* issue at **http://doi.org/10.1002/cssc.v10.19**, and the companion issue of *Energy Technology* at **http://dx.doi.org/10.1002/ente.v5.10**.

Hitherto, different n-type semiconductors were used as ETL for PSCs.[14] Subsequent work on mesoporous scaffold configurations, mostly composed of TiO_2, yielded record efficiencies up to 22.1%.[9] All subsequent PSC efficiency records were achieved using a thin (~200 nm) TiO_2 mesoporous layer as ETL except recent the P3HT-HTM-based [P3HT: poly(3-hexylthiophene-2,5-diyl)] efficiency record 16.2%, which was achieved by using a 500 nm thickness of TiO_2 scaffold layer.[15] Notably, losses owed to interfacial recombination[16] negatively affect the charge injection at the perovskite/ETL interface. Furthermore, poor charge transport of the electron (ETL)[17] and hole (HTL)[18,19] in transporting layers limit the charge collection at the working and counter electrodes, respectively. These phenomena finally lead to a reduction of the short-circuit current density (J_{SC}) and fill factor (FF).[20,21] Accordingly, owing to the highly porous nature of the mesoporous TiO_2 (mp-TiO_2) scaffold layers in PSCs, photoelectron diffusion inside the layer is slow, which leads to loss of the current by trapping the electron by regeneration reactions. There have been some efforts in the literature for improving the electron injection between the perovskite/ETL interface and electron diffusion inside the mp-TiO_2 layer by using interface engineering and different dopant materials.[22–24] However, introduction of a new type of semiconductor material, which could be fabricated by solution-based process and that has high electron diffusion behavior and high porosity, to be used as scaffold layer instead of TiO_2, is highly regarded.

Polyoxometalates (POMs) are the three-dimensional and nanosized clusters of polyatomic ions that consist of transition-metal oxyanions linked together by shared oxygen. These fascinating inorganic materials have been widely applied in various fields like catalysis, medicine, material sciences, and analytical chemistry.[25–28] This class of compounds has versatile structures with interesting redox properties, charge distribution, structure tenability, and a variety of shapes and distribution.[29,30] Among these fascinating properties, the photophysical and photochemical ones have received considerable attention.[31–33] Recently, Dong et al. successfully used a composite SiW_{12}–TiO_2 mesoporous film as ETL in PSCs.[34] Compared with the pristine TiO_2-based PSC, the SiW_{12}–TiO_2-based one showed enhanced PCE from 12.00 to 14.66%. Moreover, the SiW_{12}–TiO_2-based device also showed a good long-term stability in an ambient environment. In another work of this group, they employed a Keggin-type POM–phosphovanadomolybdate ($H_4PMo_{11}V{\cdot}n\,H_2O$) as a p-type dopant for promoting the oxidation of spiro-OMeTAD and gained the best performance with 14.05% PCE.[35] In addition, Zhang et al. used POM-induced Ostwald ripening and could successfully fabricate a hole-conductor-free fully printable PSCs with overall efficiencies of about 9.17 to 11.35% through POM molecular doping.[36]

In continuation to our previous achievement related to use of pure thin-film POM as ETL layer in dye-sensitized solar cells (DSCs),[37] herein, we successfully used a pure layer of nanoporous POM as scaffold ETL for $MAPbI_3$-based PSCs. Accordingly, in this system we used a thin layer of $[SiW_{11}O_{39}]^{8-}$, hereafter referred to as POM, instead of mp-TiO_2 as a scaffold layer for the $MAPbI_3$ perovskite layer. Owing to the high crystalline order and n-type semiconductor nature of this POM layer, electron collection on the anode is increased, which led to promising enhancement of the device photovoltaic performance.

Results and Discussion

Surface characteristics and optical properties of the POM thin film were evaluated by TEM, SEM, X-ray diffraction (XRD), UV/Vis absorbance, and diffuse reflectance spectroscopy (DRS) (see Figure 1). A TEM image from the surface of the POM layer is shown in Figure 1a. Small nanosized clusters of $[SiW_{11}O_{39}]^{8-}$ POM are orderly connected together and formed a nanoporous surface. The smooth nanoporous surface of the POM layer can be applied as a sublayer to form a well-organized perovskite layer. Furthermore, SEM images evaluated at the surface of the POM and mp-TiO_2 layers (Figure S1 in the Supporting Information) show a nanoporous structure of POM nanoparticles in comparison with the mesoporous structure of mp-TiO_2. The XRD pattern of the POM layer is also evaluated in the 2θ range of 4–80° and presented in Figure 1b. The main diffraction peak around 7.4° is correlated to (111) miller index and it is highly orientated in the direction of (111), which was previously observed in the blade-coated POM layer.[37]

The UV/Vis absorbance of the POM thin film was assessed and is shown in Figure 1c. The results show an absorbance peak in the UV region (260 nm). Furthermore, the optical absorption coefficient (α) of the POM layer was calculated using DRS data according to the Kubelka–Munk equation, $F(R)=\alpha=(1-R)^2/2R$, where R is the percentage of reflected light.[38] The incident energy of photon ($h\nu$) and the optical band gap energy (E_g) are related to the transformed Kubelka–Munk function, $[F(R)h\nu]^p=A(h\nu-E_g)$. In the calculation, the p value is set as $^1/_2$, which is correlated to the indirect allowed transition of electrons, and A is the constant that depends on transition probability. The calculation results show that the band-gap energy of the POM layer as 3.28 eV, which is in the regular range of n-type semiconductors (see Figure 1d). By using LUMO and HOMO redox potential values of SiW11 POM[39] and other interfacial layers containing c-TiO_2 (blocking layer), $MAPbI_3$, spiro-OMeTAD, gold, and FTO,[40] a general energy level diagram of the POM-based device is drawn and presented in Figure S2. The level of POM conduction bond is matched well for accepting of the perovskite-excited electron and diffusion of the electron trough the c-TiO_2 layer. The energy level of the POM and c-TiO_2 conduction bond is approximately the same (≈−4 eV), thus, diffusion of the electron from the POM/c-TiO_2 interface is physically favorable.

The statistical comparison of the J–V photovoltaic parameters were evaluated for 27 PSCs containing POM as scaffold layer and the same number PSCs using mp-TiO_2 as the scaffold layer were also evaluated. This statistical comparison is shown in Figure 2. The figure shows that the enhancement of the PCE by using POM, which can be attributed to the J_{SC} values, is promising. In addition, all the POM-based devices show V_{OC} (open-circuit voltage) values higher than 1 V whereas the mp-TiO_2-based cells show a broader range of V_{OC} values. These photovoltaic results are in agreement with our previous results

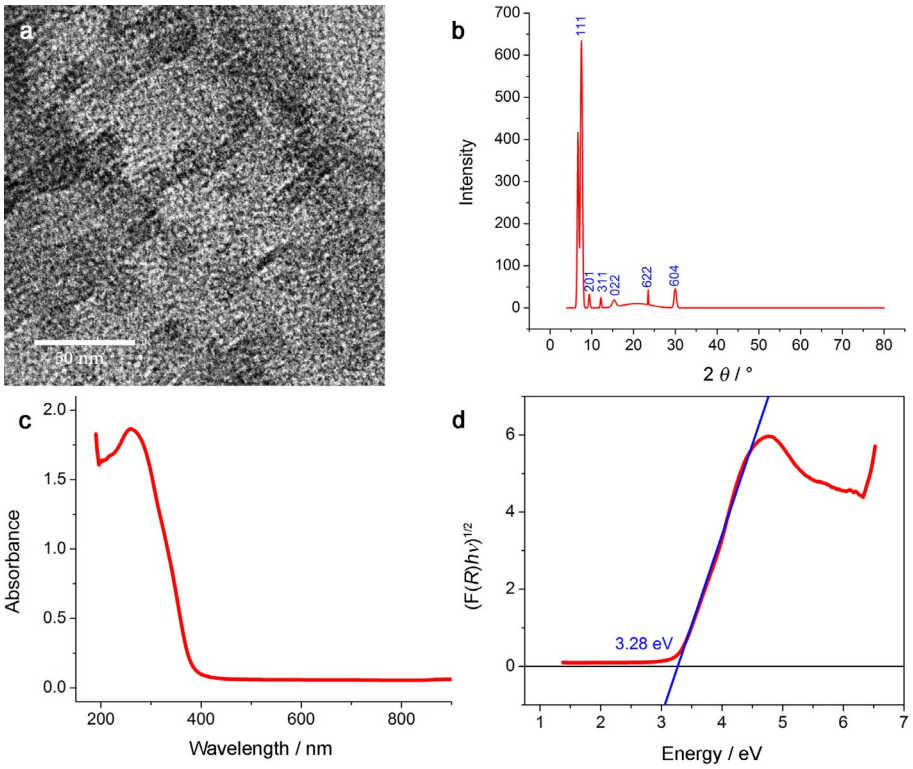

Figure 1. Surface structure and optical properties of POM thin film: a) TEM image, b) XRD pattern, c) UV/Vis absorbance, and d) transformed UV/Vis DRS spectra in the Kubelka–Munk equation, from the surface of POM layer.

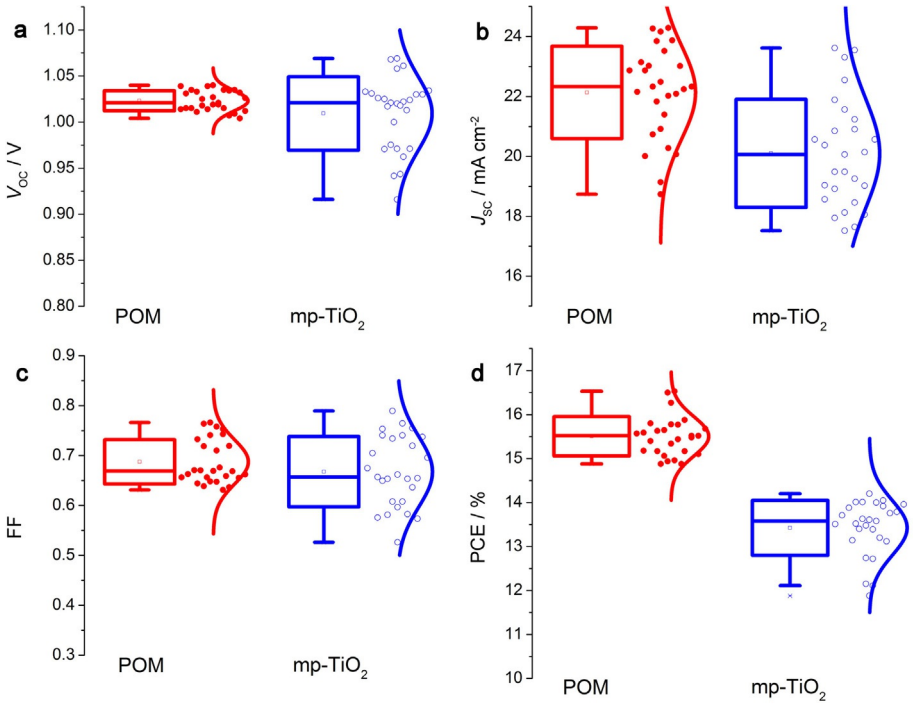

Figure 2. Statistical results of *J–V* parameters for the PSCs containing POM and mp-TiO_2 as scaffold layer. Difference of V_{OC} (a), J_{SC} (b), FF (c), and overall PCE (d) values of both device structures.

for DSCs.[37] Accordingly, high-order crystalline structure of the POM and high intrinsic electron mobility of this layer could be attributed to an increase in the photocurrent density and finally enhancement of the PCE. On the other hand, POM-based devices show higher reproducibility compared to mp-TiO_2-based PSCs. The reproducibility of the POM devices could be

well compared with highly efficient PSCs that were fabricated by interface engineering.[24] Defect-free ETL/perovskite interface causes suppresses carrier recombination in the absorber, facilitates carrier injection into the carrier transport layers, and maintains good carrier extraction at the electrodes, which finally could improve the reproducibility of the devices.

Anomalous hysteresis in the current–voltage curves is an important challenge in PSCs and resolving the hysteresis is essential for their further progress.[41] The hysteresis predominantly arises from the presence of the perovskite layer in the solar cell and it is strongly dependent on the contact material, including p- and n-type contacts, and mesoporous versus planar heterojunctions.[41] The *J*–*V* curves of the high performance PSCs of each batch is presented in both sweep directions of the bias potential (Figure 3a–b). Furthermore, photovoltaic values of corresponding *J*–*V* curves are extracted and shown in Table 1. The results clearly show that using the POM layer as scaffold in the $MAPbI_3$-based PSCs led to a significant decrease of the hysteresis in the *J*–*V* curves. As shown in the TEM image of the POM surface, a smooth nanoporous structure of this layer causes adjustment of $MAPbI_3$ nucleation and crystal growth and finally, formation of a defect-free ETL/perovskite interface.

Table 1. Photovoltaic parameters of *J*–*V* measurement in both forward and reverse voltage sweep of the perovskite solar cells containing of POM and mp-TiO_2 as scaffold layer.

Scaffold layer	Potential scan direction	V_{OC} [V]	J_{SC} [mA cm^{-2}]	FF	PCE [%]
POM	V_{OC} to 0	1.025	22.091	0.719	16.27
	0 to V_{OC}	1.007	24.05	0.667	16.15
mp-TiO_2	V_{OC} to 0	1.061	18.058	0.705	13.51
	0 to V_{OC}	1.062	19.967	0.479	10.17

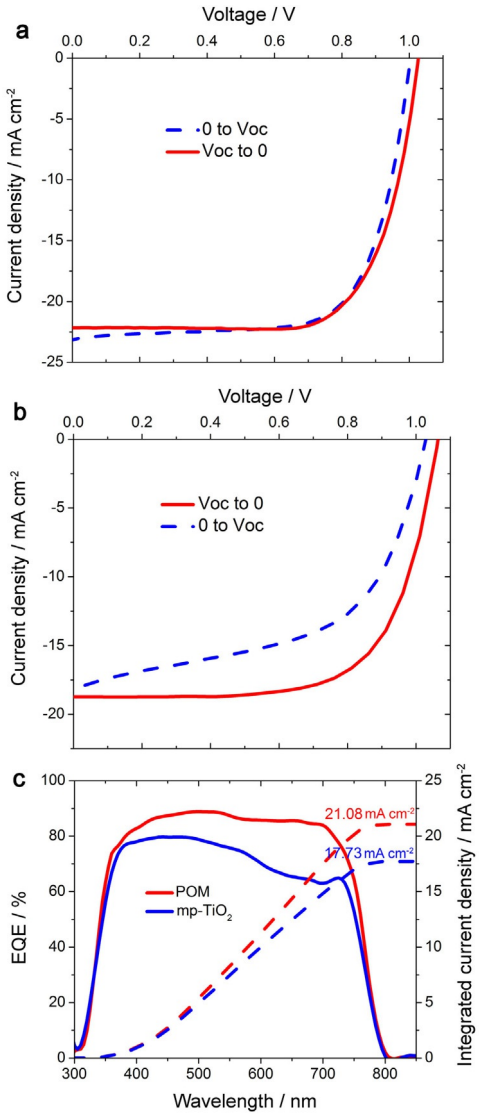

Figure 3. *J*–*V* curves of selected PSCs containing POM (a) and mp-TiO_2 (b) as scaffold layers in both forward and reverse voltage sweeps. EQE curves of the selected PSCs with comparison between POM and mp-TiO_2 scaffold layer (c).

External quantum efficiency (EQE) spectra of the high-performance PSCs are shown in Figure 3c for both POM- and mp-TiO_2-based devices. EQE integrated current density values are in good agreement with the J_{SC} values obtained by the *J*–*V* curves. In the whole range of 350–750 nm, the device containing POM as scaffold layer shows high EQE values, which generates a current density of 21.08 mA cm^{-2}. High EQE values of the POM-based device could be attributed to the defect-free ETL/perovskite interface and intrinsic high electron mobility of the POM layer. Moreover, absorbance spectra of the perovskite layer were collected and presented in Figure S3. The device containing POM as scaffold layer shows higher values of perovskite absorbance compared to the mp-TiO_2-based device. This could be attributed to more nucleation of PbI_2 and finally $MAPbI_3$ seeding on the smooth nanoporous surface of the POM layer.

To further investigate the role of the POM layer on the charge-recombination phenomena of the PSCs, V_{OC} decay measurement was performed on both POM- and mp-TiO_2-based devices. Figure 4a shows the V_{OC} decay in 100 s after cutting off the irradiation. The PSC with POM as scaffold layer shows very slow decay of V_{OC} compared with mp-TiO_2-based device. Considering that the combination of high electron mobility together with high diffusion length in POM-based PSCs implies low charge recombination at the interfaces between the perovskite layer and selective contacts,[42,16] which helps reducing the amount of recombination centers. Transients [$V(t)$] electron lifetimes in the PSCs were calculated and are shown in Figure 4b. The inset shows that the PSC with the POM scaffold layer have high τ_e values in the voltage range 0.50–0.10 V but the electron lifetimes of the PSC with mp-TiO_2 are below 0.5 s in the same voltage range. Owing to the results reported by Wang et al. for the relation between electron lifetimes and electron-transport process in a POM–TiO_2 composite by using V_{OC} decay and electrochemical impedance spectroscopy,[43] high electron lifetimes in PSCs with a POM layer could directly

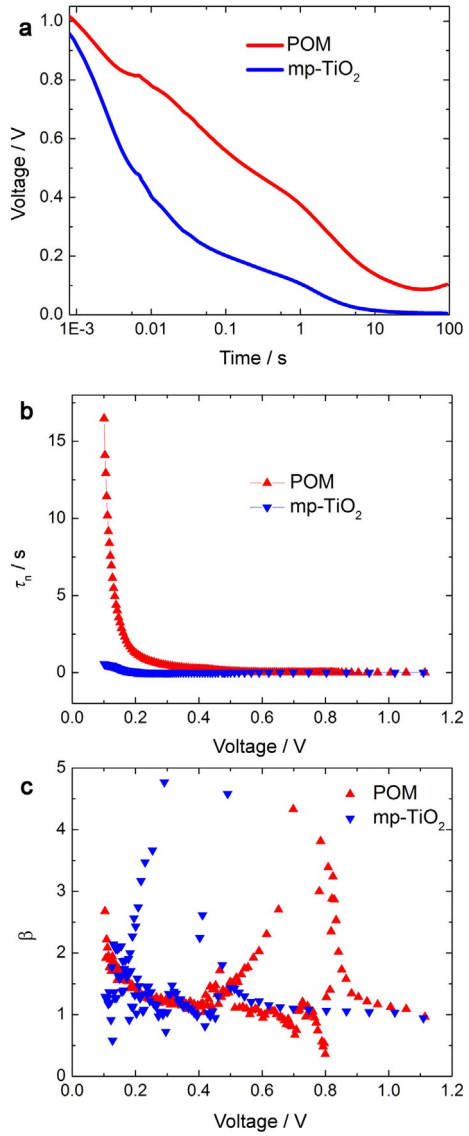

Figure 4. Experimental V_{OC} decay results of the PSCs with POM and mp-TiO_2 as scaffold layer. a) Measured $V_{OC}(t)$. b) Electron lifetime as a function of V_{OC}. c) Recombination β parameter (effective recombination order) as a function of V_{OC}.

be attributed to higher electron-transport process inside the scaffold layer.

The effective recombination order (β) was calculated using a model, including trapping effects,[44–46] and is presented in Figure 4c. Both POM- and mp-TiO_2-based devices show approximately same β values in the total range of the voltage and show a similar mechanism of electron transfer between the perovskite and ETL interface. However, there is an evident variation of the β values in the range 0.5–0.9 V for the POM-based PSC. When we make β an arbitrary function of the Fermi level, we are able to express any recombination mechanism in terms of this parameter. The β parameter is a convenient description of the lifetime dependence on the Fermi level in the device. But this parameter takes physical content (assuming it is constant) when a specific kinetic model for recombination is formulated, so a model including trapping effects in the scaffold layer is also applicable. In the case of the POM-based device, higher values of β in the range 0.5–0.9 V could be attributed to higher kinetic order of recombination mechanism, which can signify an effective recombination rate for free carriers that also counts the contribution of trapping and detrapping.[44] As the key component in efficient PSCs, the POM as ETL can selectively collect photogenerated charge carriers produced in perovskite absorbers and prevent the recombination of carriers at interfaces, thus ensuring a high PCE.

Conclusion

Here, for the first time, a pure layer of $[SiW_{11}O_{39}]^{8-}$ polyoxometalate (POM) structure was used as scaffold layer for perovskite solar cells. The POM layer was deposited by solution-based spin-coating methods and sintering at low temperature under UV irradiation. A $MAPbI_3$ perovskite layer was deposited by a sequential deposition method on the surface of the POM layer and the complete device was fabricated by spin-coating of spiro-OMeTAD and evaporation of gold as hole transport material (HTM) and counter electrode, respectively. The photovoltaic performance of the POM-based device compared to ordinary mesoporous (mp)-TiO_2-based PSC. Using of POM led to outstanding enhancement of the photocurrent density, external quantum efficiency (EQE), and overall efficiency of the PSCs. Furthermore, by changing the mp-TiO_2 to POM we could eliminate the hysteresis effect in the *J–V* curves and improve the power conversion efficiency (PCE) from 13.5 to 16.3%. The results of open-circuit voltage decay measurement show significant decrease of the electron recombination by modification of the electron transport layer/perovskite interface and higher electron transport inside the POM layer. In particular, the results introduce state-of-the-art scaffold layers, which can easily be deposited at low temperature by printing methods and would improve further fabrication of high efficient perovskite solar cells.

Experimental Section

Laser patterned FTO/glass substrates (Dyesol, 15 Ωcm^{-1}, 25 mm × 25 mm) were cleaned in an ultrasonic bath, using aqueous detergent solution, deionized water, and ethanol (15 minutes for each step). A patterned compact TiO_2 (c-TiO_2) layer was deposited onto the patterned FTO by spray pyrolysis deposition (SPD). For SPD, the substrates were fixed on a hot plate with fixed temperature at 460 °C, the spray nozzle was horizontally moved in a fixed range with 25 cm distance and 30° tilted from the substrates that positioned flat. The spray precursor solution (10 mL) was applied at each substrate's row (between 10 and 13 spray cycles). The precursor spray solution consisted of 0.16 M iisopropoxytitaniumbis(acetylacetonate) (TAA) and 0.4 M acetylacetone (ACAC) in ethanol. Patterning of the c-TiO_2 was achieved using a blade-coated metal mask.

POM $[SiW_{11}O_{39}]^{8-}$ was synthesized according to the literature.[47] Then, an appropriate paste of POM using terpineol, ethanol, and ethyl cellulose as solvents was made with a previously reported procedure.[48] The fabricated POM paste was diluted with ethanol, with a w/w ratio of 1:5, spin-coated onto the c-TiO_2 surface, and re-

leased under UV illumination of a 40 W Hg lamp for 4 h. Furthermore, for comparing the pure POM ETL with an ordinary mp-TiO_2 layer, a nanocrystalline mesoporous TiO_2 layer (18NR-T paste, Dyesol), diluted with ethanol, with w/w ratio of 1:5, was also spin-coated onto the c-TiO_2 surface and sintered using an annealing program from room temperature to 120 °C for 5 min and holding for 5 min, 120 °C to 325 °C for 15 min and holding for 5 min, 325 °C to 375 °C for 5 min and holding for 5 min, 375 °C to 480 °C for 5 min and holding for 30 min. To measure the final thickness of the POM and mp-TiO_2 layers a Dektak-Veeco 150 profilometer was used.

A sequential deposition method was selected for fabrication of the perovskite layer.[49–51] Accordingly, the lead iodide solution (PbI_2 in *N*,*N*-dimethylformamide, 500 mg mL^{-1}, 1.08 M) was deposited by a spin-coating technique at 6000 rpm for 10 s with 6000 as acceleration rate on the surface of POM and mp-TiO_2 substrates and then annealed at 70 °C for 5 min. $CH_3NH_3PbI_3$ crystallization was achieved by dipping the PbI_2 layers in a methylammonium iodide solution (CH_3NH_3I in 2-propanol 10 mg mL^{-1}) for 10 min, washing immediately with 2-propanol by spin-coating at 6000 rpm with 6000 as acceleration rate for 10 s and dried at 110 °C for 10 min.

The HTLs were deposited by spin-coating spiro-OMeTAD solution (73.2 mg mL^{-1}) on top of the perovskite layer. The spiro-OMeTAD was deposited by spin-coating at 2000 rpm for 20 s and 2000 as acceleration rate. The spiro-OMeTAD solution was doped by 7.2 µl of cobalt 209 (stock solution 375 mg in 1 mL acetonitrile), 11.4 µl of tert-butylpyridine (TBP), and 12 µl of lithium bis(trifluoromethanesulfonyl)imide (LiTFSI) solution (520 mg in 1 mL of acetonitrile). The thickness of all samples was measured with a profilometer (DektakVeeco 150). Samples were introduced into a high-vacuum chamber (10^{-6} mbar) to thermally evaporate the Au back contacts (thickness 100 nm). Here, layer deposition for all layers was performed under ambient condition.

Powder X-ray diffraction (XRD) patterns of the samples were recorded on a Bruker, D8 ADVANCE, Germany, wavelength: 1.5406 Å (CuK_α), voltage: 40 kV, current: 40 mA in the 2θ range from 4 to 80°. UV/Vis diffuse reflectance spectra (UV/Vis/DRS) were recorded on a UV/Vis spectrophotometer, JASCO, V-670 (190–2700 nm), Japan using $BaSO_4$ as a reference.

J–*V* characteristics of masked devices were tested with a solar simulator (KSRI, Model 1010, class A) giving AM1.5G illumination, which was calibrated using a certified reference solar cell (Fraunhofer ISE) at an intensity 1000 W m^{-2}. PSC measurements were performed following the suggestion given in Refs. [52], [53]. EQE spectra were recorded using a computer-controlled setup consisting of a Xe light source (Nikon Xenon XE High Intensity Light Lamp), a monochromator (Spectral Products CM110 Compact 1/8 Meter), and a potentiostat (Autolab 302N), calibrated using a certified reference solar cell (Fraunhofer ISE). The morphology and grain size of the POM, PbI_2, and perovskite layers were obtained using TEM (TEM ZEISS). V_{OC} decay measurements were performed with a 100 W white LED irradiation and probing the voltage using the Autolab 302N potentiostat.

Acknowledgements

The authors wish to thank the Islamic Azad University of Shahrekord and Kimia Solar Company for financially supporting of this work.

Conflict of interest

The authors declare no conflict of interest.

Keywords: keggin type · lead halide · perovskite solar cell · polyoxometalate · scaffold layer

[1] M. M. Lee, J. Teuscher, T. Miyasaka, T. N. Murakami, H. J. Snaith, *Science* **2012**, *338*, 643.
[2] H. S. Kim, C. R. Lee, J. H. Im, K. B. Lee, T. Moehl, A. Marchioro, S. J. Moon, R. Humphry-Baker, J. H. Yum, J. E. Moser et al., *Sci. Rep.* **2012**, *2*, 1.
[3] S. De Wolf, J. Holovsky, S. J. Moon, P. Löper, B. Niesen, M. Ledinsky, F. J. Haug, J. H. Yum, C. Ballif, *J. Phys. Chem. Lett.* **2014**, *5*, 1035.
[4] W. S. Yang, J. H. Noh, N. J. Jeon, Y. C. Kim, S. Ryu, J. Seo, S. I. Seok, *Science* **2015**, *348*, 1234.
[5] W. J. Yin, T. Shi, Y. Yan, *Adv. Mater.* **2014**, *26*, 4653.
[6] M. A. Green, A. Ho-Baillie, H. J. Snaith, *Nat. Photonics* **2014**, *8*, 506.
[7] D. Shi, V. Adinolfi, R. Comin, M. Yuan, E. Alarousu, A. Buin, Y. Chen, S. Hoogland, A. Rothenberger, K. Katsiev, Y. Losovyj, X. Zhang, P. A. Dowben, O. F. Mohammed, E. H. Sargent, O. M. Bakr, *Science* **2015**, *347*, 519.
[8] S. D. Stranks, G. E. Eperon, G. Grancini, C. Menelaou, M. J. P. Alcocer, T. Leijtens, L. M. Herz, A. Petrozza, H. J. Snaith, *Science* **2013**, *342*, 341.
[9] National Renewable Energy Laboratory (NREL) Efficiency Chart, http://www.nrel.gov/ncpv/images/efficiency_chart.jpg (accessed on 28th May 2017).
[10] A. Marchioro, J. Teuscher, D. Friedrich, M. Kunst, R. van de Krol, T. Moehl, M. Grätzel, J.-E. Moser, *Nat. Photonics* **2014**, *8*, 250.
[11] E. Edri, S. Kirmayer, S. Mukhopadhyay, K. Gartsman, G. Hodes, D. Cahen, *Nat. Commun.* **2014**, *5*, 3461.
[12] V. Gonzalez-Pedro, E. J. Juarez-Perez, W. S. Arsyad, E. M. Barea, F. Fabregat-Santiago, I. Mora-Sero, J. Bisquert, *Nano Lett.* **2014**, *14*, 888.
[13] E. J. Juarez-Perez, M. Wußler, F. Fabregat-Santiago, K. Lakus-Wollny, E. Mankel, T. Mayer, W. Jaegermann, I. Mora-Sero, *J. Phys. Chem. Lett.* **2014**, *5*, 680.
[14] N. Marinova, S. Valero, J. L. Delgado, *J. Colloid Interface Sci.* **2017**, *488*, 373.
[15] N. Y. Nia, F. Matteocci, L. Cina, A. Di Carlo, *ChemSusChem* **2017**, DOI: https://doi.org/10.1002/cssc.201700635.
[16] J. M. Marin-Beloqui, L. Lanzetta, E. Palomares, *Chem. Mater.* **2016**, *28*, 207.
[17] E. M. Hutter, G. E. Eperon, S. D. Stranks, T. J. Savenije, *J. Phys. Chem. Lett.* **2015**, *6*, 3082.
[18] A. Agresti, S. Pescetelli, S. Casaluci, *IEEE International Conference on Nanotechnology*; Rome, Italy, **2015**, 732.
[19] Y. Wang, H.-Y. Wang, M. Yu, L. Fu, Y. Qin, J.-P. Zhang, X. Ai, *Phys. Chem. Chem. Phys.* **2015**, *17*, 29501.
[20] K. Sveinbjörnsson, K. Aitola, X. Zhang, M. Pazoki, A. Hagfeldt, G. Boschloo, E. M. J. Johansson, *J. Phys. Chem. Lett.* **2015**, *6*, 4259.
[21] A. Listorti, E. J. Juarez-Perez, C. Frontera, V. Roiati, L. Garcia-Andrade, S. Colella, A. Rizzo, P. Ortiz, I. Mora-Sero, *J. Phys. Chem. Lett.* **2015**, *6*, 1628.
[22] A. Bera, A. D. Sheikh, M. A. Haque, R. Bose, E. Alarousu, O. F. Mohammed, T. Wu, *ACS Appl. Mater. Interfaces* **2015**, *7*, 28404.
[23] A. Agresti, S. Pescetelli, B. Taheri, A. E. Del Rio Castillo, L. Cina, F. Bonaccorso, A. Di Carlo, *ChemSusChem* **2016**, *9*, 2609.
[24] H. Zhou, Q. Chen, G. Li, S. Luo, T. Song, H. S. Duan, Z. Hong, J. You, Y. Liu, Y. Yang, *Science* **2014**, *345*, 542.
[25] M. T. Pope, A. Müller, *Angew. Chem. Int. Ed. Engl.* **1991**, *30*, 34; *Angew. Chem.* **1991**, *103*, 56.
[26] J. T. Rhule, C. L. Hill, D. A. Judd, *Chem. Rev.* **1998**, *98*, 327.
[27] H. Park, W. Choi, *J. Phys. Chem. B* **2003**, *107*, 3885.
[28] Z. X. Sun, L. Xu, W. H. Guo, B. B. Xu, S. P. Liu, F. Y. Li, *J. Phys. Chem. C* **2010**, *114*, 5211.
[29] N. V. Izarova, M. T. Pope, U. Kortz, *Angew. Chem. Int. Ed.* **2012**, *51*, 9492; *Angew. Chem.* **2012**, *124*, 9630.
[30] X. P. Zheng, Y. Lu, H. Zhang, Z. M. Zhang, E. B. Wang, *Inorg. Chem. Commun.* **2013**, *33*, 29.

[31] Z. Wang, Y. Ma, R. Zhang, A. Peng, Q. Liao, Z. Cao, H. Fu, J. Yao, *Adv. Mater.* **2009**, *21*, 1737.
[32] L. Wang, L. Xu, Z. Mu, C. Wang, Z. Sun, *J. Mater. Chem.* **2012**, *22*, 23627.
[33] J. J. Walsh, A. M. Bond, R. J. Forster, T. E. Keyes, *Coord. Chem. Rev.* **2016**, *306*, 217.
[34] G. Dong, T. Ye, Y. Yang, L. Sheng, D. Xia, J. Wang, X. Fan, R. Fan, *ChemSusChem* **2017**, *10*, 2218.
[35] G. Dong, D. Xia, Y. Yang, L. Shenga, T. Ye, R. Fan, *ACS Appl. Mater. Interfaces* **2017**, *9*, 2378.
[36] Y. Zhang, Y. Wang, Z. Sun, F. Li, R. Tao, Z. Jin, L. Xu, *Chem. Commun.* **2017**, *53*, 2290.
[37] D. Karimian, B. Yadollahi, M. Zendehdel, V. Mirkhani, *RSC Adv.* **2015**, *5*, 76875.
[38] H. Lin, C. P. Huang, W. Li, C. Ni, S. I. Shah, Y.-H. Tseng, *Appl. Catal. B* **2006**, *68*, 1.
[39] J.-S. Li, X.-J. Sang, W.-L. Chen, L.-C. Zhang, Z.-M. Zhu, T.-Y. Ma, Z.-M. Su, E.-B. Wang, *ACS Appl. Mater. Interfaces* **2015**, *7*, 13714.
[40] Y. Song, S. Lv, X. Liu, X. Li, S. Wang, H. Wei, D. Li, Y. Xiao, Q. Meng, *Chem. Commun.* **2014**, *50*, 15239.
[41] H. J. Snaith, A. Abate, J. M. Ball, G. E. Eperon, T. Leijtens, N. K. Noel, S. D. Stranks, J. T. W. Wang, K. Wojciechowski, W. Zhang, *J. Phys. Chem. Lett.* **2014**, *5*, 1511.
[42] Y. H. Lee, J. Luo, M. K. Son, P. Gao, K. T. Cho, J. Seo, S. M. Zakeeruddin, M. Grätzel, M. K. Nazeeruddin, *Adv. Mater.* **2016**, *28*, 3966.
[43] S.-M. Wang, L. Liu, W.-L. Chen, E.-B. Wang, Z.-M. Su, *Dalton Trans.* **2013**, *42*, 2691.
[44] A. Zaban, M. Greenshtein, J. Bisquert, *ChemPhysChem* **2003**, *4*, 859.
[45] M. H. Habibi, B. Karimi, M. Zendehdel, M. Habibi, *J. Ind. Eng. Chem.* **2014**, *20*, 1462.
[46] M. H. Habibi, B. Karimi, M. Zendehdel, M. Habibi, *Spectrochim. Acta Part A* **2013**, *116*, 374.
[47] P. Souchay, *Polyanions et Polycations*; Gauthier-Villars: Paris, **1963**.
[48] M. H. Habibi, M. Mikhak, M. Zendehdel, M. Habibi, *Int. J. Electrochem. Sci.* **2012**, *7*, 6787.
[49] J. Burschka, N. Pellet, S.-J. Moon, R. Humphry-Baker, P. Gao, M. K. Nazeeruddin, M. Grätzel, *Nature* **2013**, *499*, 316.
[50] Y. Zhou, M. Yang, A. L. Vasiliev, H. F. Garces, Y. Zhao, D. Wang, S. Pang, K. Zhu, N. P. Padture, *J. Mater. Chem. A* **2015**, *3*, 9249.
[51] T. Liu, Q. Hu, J. Wu, K. Chen, L. Zhao, F. Liu, C. Wang, H. Lu, S. Jia, T. Russell, R. Zhu, Q. Gong, *Adv. Energy Mater.* **2016**, *6*, 1501890.
[52] E. Zimmermann, P. Ehrenreich, T. Pfadler, J. A. Dorman, J. Weickert, L. Schmidt-Mende, *Nat. Photonics* **2014**, *8*, 669.
[53] J. A. Christians, J. S. Manser, P. V. Kamat, *J. Phys. Chem. Lett.* **2015**, *6*, 852.

Manuscript received: June 9, 2017
Revised manuscript received: July 5, 2017
Accepted manuscript online: July 7, 2017
Version of record online: August 21, 2017